Journal of Molecular Liquids 446 (2026) 129210

Contents lists available at ScienceDirect

Journal of Molecular Liquids

journal homepage: www.elsevier.com/locate/molliq

Self-diffusion in ferrogranulates: Stockmayer model revisited

Oksana Bilous[a], Kirill A. Okrugin[a], Ali Lakkis[b], Reinhard Richter[b], Sofia Kantorovich[a,*]

[a] University of Vienna, Faculty of Physics, Kolingasse 14-16, Vienna, Austria
[b] University of Bayreuth, Experimental Physics 5, Universitätsstrasse 30, Bayreuth, Germany

HIGHLIGHTS

- A quasi-2D mixture of Stockmayer dipolar and repulsive particles is analysed using large-scale Langevin dynamics simulations.
- The combined effects of area fraction, dipolar interactions, and out-of-plane magnetic fields on clustering and dynamics are quantified.
- Without induction, isolated particles show Gaussian diffusion, while crowding causes subdiffusion and stronger non-Gaussianity.
- Strong magnetic induction restructures dipolar aggregates and indirectly slows down the diffusion of non-magnetic particles, producing a “magnetic cooling” effect.
- The results provide a framework for interpreting structure-diffusion coupling.

ARTICLE INFO

Keywords:
Magnetic multicore nanoparticles
Dynamic magnetic susceptibility
Magnetic anisotropy
Specific loss power
Brownian dynamics

ABSTRACT

We present a systematic numerical study of a quasi-two-dimensional mixed system composed of Stockmayer-type dipolar particles and purely repulsive non-polar particles. By combining detailed cluster analysis with a quantitative evaluation of self-diffusion, we demonstrate how the interplay between particle area fraction, dipolar interactions, and an out-of-plane magnetic induction governs the structural organisation and dynamical behaviour of the mixture. We show that, in the absence of induction, isolated magnetic particles diffuse essentially in a Gaussian manner across all concentrations. At longer time scales, by contrast, the system enters a crowding-dominated diffusive regime, in which both the diffusion exponent and the non-Gaussianity vary monotonically with area fraction. Our findings provide a framework for interpreting diffusion phenomena in ferrogranular materials and pave the way for future experimental verification, particularly regarding induction-controlled cooling of non-magnetic components.

1. Introduction

The study of self-diffusion in liquids remains a central topic in condensed matter and statistical physics, as it provides a direct connection between microscopic particle motion and macroscopic transport properties [1–6]. Self-diffusion reflects the interplay between thermal fluctuations and interparticle interactions; therefore, it serves as a sensitive probe of the local structure and dynamics of molecular and complex fluids [7–9]. Understanding how microscopic interactions influence diffusive behaviour is essential for describing the dynamical response of liquids across a broad range of conditions [10,11].

More than eight decades have passed since the seminal work of Stockmayer [12], who introduced a model fluid composed of particles interacting through a combination of Lennard-Jones (1) and dipole-dipole (2) potentials. The first is given by

$$u_{ij}^{\mathrm{LJ}} = 4\varepsilon\left[\left(\frac{\sigma}{r_{ij}}\right)^{12} - \left(\frac{\sigma}{r_{ij}}\right)^{6}\right], \tag{1}$$

where $\vec{r}_{ij}$, with $|\vec{r}_{ij}| = r_{ij}$, is the vector connecting the centres of particles (or molecules) i and j. The parameter σ represents the characteristic particle size, while ε sets the energy scale, *i.e.*, the depth of the potential well or the strength of attraction between particles. The dipole-dipole potential has a form

$$u_{ij}^{\mathrm{DD}} = \mu^{*}\left[\frac{\vec{m}_i \cdot \vec{m}_j}{r_{ij}^{3}} - 3\frac{(\vec{m}_i \cdot \vec{r}_{ij})(\vec{m}_j \cdot \vec{r}_{ij})}{r_{ij}^{5}}\right], \tag{2}$$

where $\vec{m}_i$ and $\vec{m}_j$ are the dipole moments of particles i and j, respectively, and μ^{*} is a constant that determines the strength of the dipole-dipole interaction.

* Corresponding author.
Email addresses: oksana.bilous@univie.ac.at (O. Bilous), sofia.kantorovich@univie.ac.at (S. Kantorovich).

https://doi.org/10.1016/j.molliq.2025.129210
Received 3 December 2025; Accepted 27 December 2025
Available online 9 January 2026

The Stockmayer fluid has since become a cornerstone of molecular simulation studies [13–17], offering a simple yet powerful framework for describing a wide variety of systems, including polar liquids and dipolar gases.

Subsequent studies have shown that the Stockmayer description can also be extended to ferrofluids, provided that the magnetic and thermodynamic parameters lie within appropriate ranges [18–21]. Over the years, it has been demonstrated that the Stockmayer model effectively captures the essential features of systems characterised by (sub)nanometer-scale interactions, where short-range repulsion and long-range dipolar attraction together determine both equilibrium and dynamical properties.

More recently, it has been demonstrated that analogous concepts may even be applied to ferrogranular materials [22,23], in which millimetre-sized magnetic grains display collective behaviour reminiscent of their nanoscale counterparts. This conceptual continuity underscores the universality of dipolar interaction models and motivates their application to systems extending well beyond the nanoscale. In our previous work, we have shown that the Stockmayer-type model successfully describes features of ferrogranular systems [24–26]. While direct experimental access to self-diffusion in these materials remains challenging and is the subject of ongoing efforts, numerical simulations provide a powerful means to predict and interpret diffusive dynamics under well-controlled conditions.

While diffusion in Stockmayer and dipolar fluids has been widely investigated [27–34], the specific case of a mixed system comprising non-polar (purely repulsive) and polar (attractive and dipolar) particles confined to a quasi-two-dimensional (q2D) geometry has not yet been systematically explored. Such a mixture may be regarded as a zeotropic system, akin to previously studied Stockmayer mixtures in which the non-polar component was still represented by a Lennard-Jones fluid with an attractive interaction [21].

In the present work, however, we focus on a system with distinct interaction characteristics, offering a new perspective on clustering phenomena and transport processes in confined Stockmayer systems mixed with non-polar, non-sticky purely repulsive particles, aiming to embrace the diffusion in ferrogranulate layers as well.

The remainder of this paper is organised as follows. In the next Section 2, we introduce the computational methodology, outline the system parameters, and define the principal observables. Section 3 is divided into three parts: first, we analyse the formation and morphology of clusters formed by magnetic particles; second, we characterise the self-diffusive behaviour of the system; third, we analyse the non-Gaussianity of particles in the system. The manuscript concludes with a brief summary of the main results and an outlook for future research.

2. Methods

This section describes the model (Section 2.1), the simulation protocol (Section 2.2) and the estimation of the mean square displacement (Section 2.3).

2.1. Model

We consider two types of particles placed in a laterally periodic square simulation box with a constant side, at a constant temperature, T. All particle centres are confined to one plane, but rotations are possible in all three dimensions.

Particle details. Magnetic particles are modelled as a Stockmayer system described by Eqs. (1)–(2) with $\varepsilon = \varepsilon_{\mathrm{m}} = 0.5$; dimensionless particle size $\sigma = \sigma_{\mathrm{m}} = 3$; $\mu^* = \mu_0/4\pi$, where μ_0 is the magnetic permeability of vacuum; and $m^2/k_B T\sigma_{\mathrm{m}}^3 = 10$. In dimensionless simulation units $k_B T = 0.5$. The thermal energy is chosen to be low in order to allow for the granular athermal character of ferrogranulates [35].

Pure repulsive particles (glass beads in a ferrogranulate) are characterised by a dimensionless diameter of $\sigma_{\mathrm{g}} = 4$, with interactions governed by the Weeks-Chandler-Andersen (WCA) potential:

$$u_{ij}^{\mathrm{WCA}} = \begin{cases} u_{\mathrm{LJ}}(r_{ij}) - u_{\mathrm{LJ}}(r_{\mathrm{cut}}), & r_{ij} < r_{\mathrm{cut}} \\ 0, & r_{ij} \geq r_{\mathrm{cut}} \end{cases}. \tag{3}$$

Here, $\varepsilon = 10$ and $r_{\mathrm{cut}} = 2^{1/6}\sigma_{\mathrm{g}}$ [36].

The interactions between glass and magnetic beads are modelled using the Weeks-Chandler-Andersen potential (3) with the same $\varepsilon = 10$. The effective diameter, denoted as $\sigma = (\sigma_{\mathrm{m}} + \sigma_{\mathrm{g}})/2$, is used with an appropriate cutoff radius $r_{\mathrm{cut}} = 2^{1/6}\sigma$.

The total area fraction of particles, ϕ_n, is the sum of the area fractions of magnetic, ϕ_{m}, and purely repulsive (glass for a ferrogranulate) beads, ϕ_{g}:

$$\phi_n = \phi_{\mathrm{m}} + \phi_{\mathrm{g}}. \tag{4}$$

The area fractions for magnetic/glass beads, respectively, are estimated by

$$\phi_{\mathrm{m/g}} = \frac{N_{\mathrm{m/g}}\pi\sigma_{\mathrm{m/g}}^2}{4L^2},$$

where $N_{\mathrm{m/g}}$ denotes the number of spheres enclosed in a square simulation box with a side length of $L = 240$. The list of investigated area fractions is detailed in Table 1. The numbers of magnetic, N_{m}, and glass, N_{g}, beads were varied. The area fractions in Table 1 are chosen in such a way that the ratio between the magnetic and nonmagnetic components is preserved and is equal to $\phi_{\mathrm{m}}/\phi_{\mathrm{g}} \sim 1.3$. Keeping the ratio constant facilitates a deeper understanding of the impact of ϕ_n without mixing in the influence of other factors.

Table 1
The overall area fraction ϕ_n, along with the magnetic particles ϕ_{m} and glass particles ϕ_{g}, is used in Figs. 1 and 2.

	ϕ_n	ϕ_{m}	ϕ_{g}
ϕ_1	0.175	0.100	0.075
ϕ_2	0.210	0.120	0.090
ϕ_3	0.233	0.133	0.100
ϕ_4	0.268	0.153	0.115
ϕ_5	0.300	0.170	0.130
ϕ_6	0.303	0.173	0.130
ϕ_7	0.315	0.180	0.135
ϕ_8	0.350	0.200	0.150

Particle masses, inertia tensors, and dimensionless friction coefficients, γ are all set to unity, as the focus lies on steady-state behavior and the relative effects of particle area fraction and applied induction.

Magnetic induction. To evaluate the impact of an external magnetic induction $\vec{B}^*$, we apply it orthogonal to the layer of the particles. $\vec{B}^*$ tends to align each magnetic particle dipole moment $\vec{m}_i$ with its direction out-of-the-plane through the Zeeman energy:

$$u_i^Z = -\left(\vec{m}_i \cdot \vec{B}^*\right). \tag{5}$$

The dimensionless values of the induction are scaled such that the Langevin parameter, $mB^*/k_{\mathrm{B}}T$, takes values of 0, $\sqrt{5}$, and $2\sqrt{5}$, leading to three dimensionless magnitudes of the applied out-of-plane induction: $|\vec{B}_0^*| = 0.0$, $|\vec{B}_1^*| = 0.5$, and $|\vec{B}_2^*| = 1.0$. These values correspond to low, intermediate, and nearly saturating effects on the orientation of magnetic particles in ferrogranulates [26].

2.2. Simulation protocol

We employ Langevin dynamics in a quasi-2D geometry to model a two-component mixture, incorporating the interactions and dimensionless parameters described earlier [37].

The system was equilibrated for 60×10^6 integration steps. Equilibrium was defined based on the stability of the cluster size distribution, where clusters were identified using an energy–distance criterion [38]: two particles were considered part of the same cluster if their pair interaction energy was negative and their separation did not exceed 30% above the contact distance. Once the cluster size distribution reached a steady state, exhibiting no significant temporal fluctuations (less than 10%), the system was considered equilibrated.

It should be noted that, in dense systems and in the absence of an external magnetic field, the resulting clusters may represent kinetically trapped but steady configurations. Nevertheless, even under such conditions, the main results of this study remain valid.

After equilibration, production runs of 20×10^3 integration steps were carried out. During this stage, cluster configurations were stored at regular intervals, and particles were classified as either permanently single or as attaching/detaching from clusters during the observation period. Simultaneously, the mean-square displacement (MSD) was computed.

For statistical purposes, for each value of ϕ_n (Table 1) and $|\vec{B}^*_n|$, eight independent runs were performed.

Throughout the entire duration of the simulations, the time-step maintains a constant value of $\delta t = 0.0005$.

These simulations were executed using the ESPResSo 4.1.4 simulation package, employing the velocity Verlet algorithm [39] for solving Langevin equations, and the P3M method [40] combined with dipolar layer correction [41] for calculating long range magnetic forces in a not fully periodic system.

2.3. Determination of the mean-square displacement

The mean-square displacement MSD as a function of time lag τ is calculated as:

$$\langle \Delta r^2(\tau) \rangle = \langle [r(t+\tau) - r(t)]^2 \rangle, \tag{6}$$

where $r(t)$ is the position of a particle at time t, and $\langle \cdot \rangle$ denotes an ensemble average.

For a system in equilibrium, the MSD can be described by the following equation, which gives the dimension of the MSD in terms of the diffusion coefficient D [2]:

$$\langle \Delta r^2(\tau) \rangle = 4D\tau^{\alpha}, \tag{7}$$

where α is the scaling exponent. If $\alpha \sim 1$, we are dealing with standard Brownian diffusion, while for exponents different from unity, the diffusion is usually referred to as anomalous. In general, the value of α can vary depending on the interparticle interactions. The diffusion coefficient D is then defined as:

$$D = \frac{\langle \Delta r^2(\tau) \rangle}{4\tau^{\alpha}}. \tag{8}$$

To compute MSD, we used a Python implementation that takes advantage of the tidynamics library [42]. It is convenient to analyse the dimensionless diffusion coefficient, D/D_0, where $D_0 = k_B T/\gamma$, with k_B denoting the Boltzmann constant and γ being the friction coefficient.

Alongside the anomalous diffusion exponent obtained from the MSD scaling, the nature of diffusion can also be characterised by examining whether the underlying displacement statistics are Gaussian or non-Gaussian. This distinction is determined from the probability distribution of particle displacements, $P(\delta x, t)$, evaluated at different lag times t. Numerous soft-matter systems exhibit combinations such as Gaussian but non-Brownian diffusion or Brownian yet non-Gaussian diffusion, reflecting the complexity of their underlying dynamics (see, [43] and references therein). In the present work, we likewise computed the displacement distribution over the same time interval used for the MSD analysis, allowing us to assess both the anomalous exponent and the Gaussian/non-Gaussian character of particle motion.

3. Results and discussions

This section starts with a cluster analysis (Section 3.1), which is followed by an estimation of the self-diffusion (Section 3.2).

3.1. Cluster analysis

Initially, we conducted a visual assessment of the equilibrium states that our systems adopted during the simulations, as depicted in Fig. 1.

In these snapshots, glass particles are shown in gray, while magnetic particles are represented in dark red, each with a dark blue hemisphere indicating the orientation of the magnetic moment. The snapshots reflect three distinct magnitudes of the applied magnetic induction ($|\vec{B}^*_{zn}|$) and three corresponding total area fractions of particles. Moving from left to right in Fig. 1, we observe an increase in the particle area fraction, as detailed in Table 1.

The present observations align well with the conclusions reported previously [25,26]. In the absence of an external magnetic induction (bottom row), the increase in ϕ_n leads to the formation of larger clusters. However, no significant qualitative changes in the structure or the emergence of new aggregation patterns appear. These results corroborate the findings of researchers investigating the self-assembly of magnetic particles released from a steel plate [44], in liquid media [45], as well as the clustering phenomena observed in granular systems, which display a liquid-solid-like phase transition under out-of-equilibrium conditions [46].

Examining the column on the right-hand side, corresponding to the maximum value of ϕ_n, indicates a consistent pattern: irrespective of the magnitude of $|\vec{B}^*|$, the overall structure of the aggregate is preserved. Specifically, it exhibits a hexagonal local arrangement where particles align in a head-to-tail configuration, forming chains that are offset by half a particle. As $|\vec{B}^*|$ increases (see rows 2 and 3 in Fig. 1), the fraction of isolated magnetic particles that align their magnetic moments with the field also rises. This leads to a configuration characterised by dipole-dipole repulsion, which cannot be offset by dipolar in-plane favourable head-to-tail attraction at low particle area fractions. This becomes prominent in the top left quadrant (minimal ϕ_n and maximal B^*), where the majority of magnetic particles are non-aggregated. Likewise,

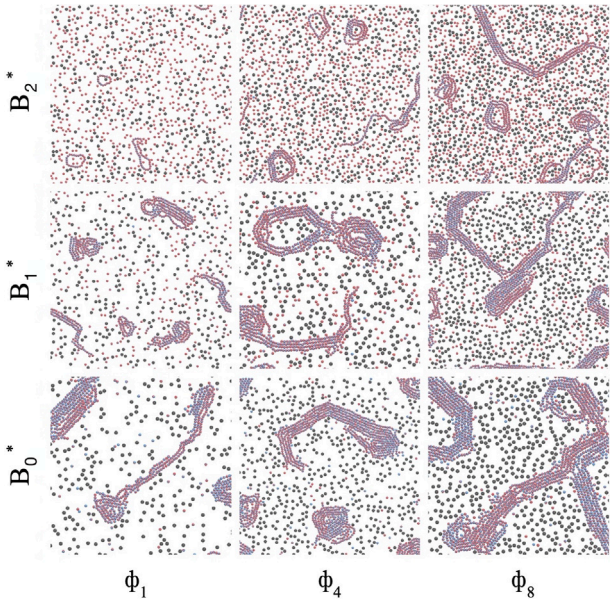

Fig. 1. Typical simulation snapshots. The total area fraction ϕ_n from left to right: $\phi_1 = 0.175$, $\phi_4 = 0.268$, $\phi_8 = 0.350$. The applied external magnetic induction grows from bottom to top $|\vec{B}^*_0| = 0.0$, via $|\vec{B}^*_1| = 0.5$, to $|\vec{B}^*_2| = 1.0$, in simulation units.

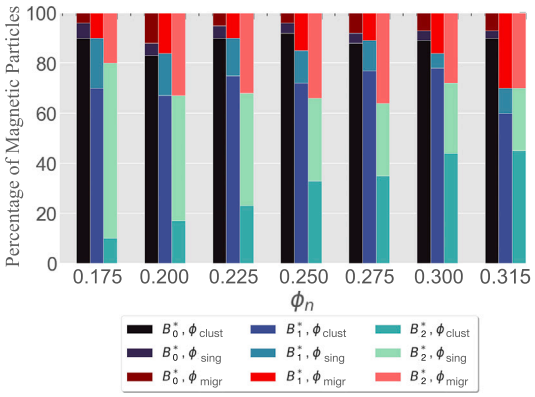

Fig. 2. The fraction of magnetic particles (%) within clusters, ϕ_{clus}, single particles, ϕ_{sing}, and particles migrating from a clustered to a single state (or reverse), ϕ_{migr} *versus* total area fraction ϕ_n. In each column, the magnetic induction changes from 0.0 to 1.0 in simulation units.

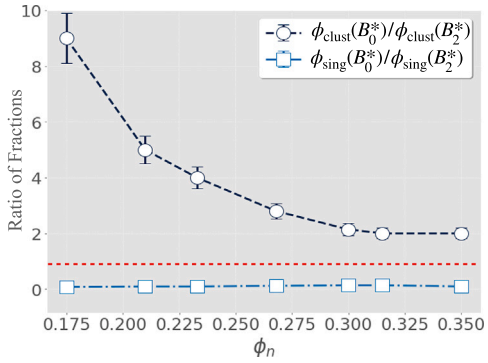

Fig. 3. Dependence of $\phi_{\text{clus}}(B_0^*)/\phi_{\text{clus}}(B_2^*)$ (circles, black) and $\phi_{\text{sing}}(B_0^*)/\phi_{\text{sing}}(B_2^*)$ (squares, light blue) *versus* total area fraction, ϕ_n. Red dashed horizontal line marks unity. Vertical lines around symbols, if seen, show error-bars.

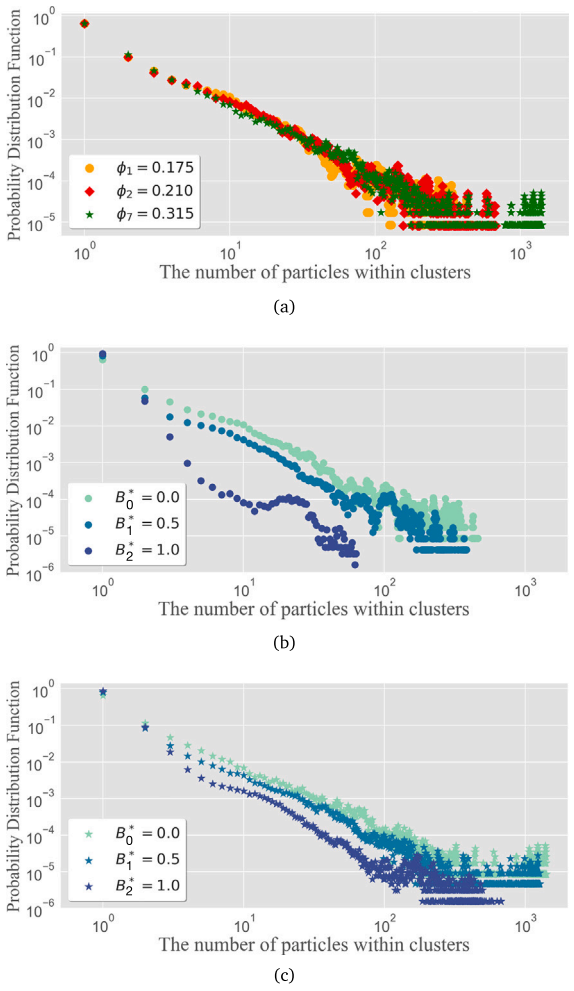

Fig. 4. Probability distribution function (PDF) of the number of particles within clusters as a function of cluster size for different magnetic induction strengths B^*, at a constant total area fraction. (a) compares three area fractions in the absence of magnetic induction. Panel (b) shows results for $\phi_1 = 0.175$, while (c) illustrates $\phi_7 = 0.315$. Three curves in (b) and (c) are for three values of magnetic induction B^* as shown in the legend.

in its diagonal counterpart, the bottom right quadrant for the high value of ϕ_n and no applied induction evidences the formation of large clusters. The structures observed in the simulation snapshots are similar to the experimental findings in [25].

To quantify the observations, in Fig. 2, we show how the percentage of magnetic particles in clusters, ϕ_{clus}, single particles, ϕ_{sing}, and migrating particles, ϕ_{migr}, depends on the area fraction and the strength of the magnetic induction.

As the induction strength increases, ϕ_{clus} decreases. This can be seen by comparing the three bars within each value of ϕ_n: the black bars are consistently higher than the dark blue and dark turquoise bars, especially at intermediate particle concentration. In contrast, both the migrating and single-particle fractions grow with increasing B^*. For migrating particles, this is shown by the bars in progressively darker to lighter shades of red; for single particles, by the central bars in each column, which shift from dark purple to light blue and finally to light turquoise, as indicated in the legend. The actual values of the area fractions of clustered, single, and migrating magnetic particles are collected in Table. S1 in the Supplementary.

To further examine how the combined increase in B^* and ϕ_n affects cluster formation, Fig. 3 shows the ratio between the fraction of clustered particles in the absence of induction and that at the highest applied B^* (circles). At low area fractions, the system contains nearly ten times more clustered particles when no induction is applied; however, this ratio decreases to about two at high area fractions. Interestingly, the corresponding ratio for the fraction of single particles (squares) is essentially insensitive to ϕ_n: at zero applied induction, only very few particles remain single, whereas at finite B^*, the combined fraction of migrating and single particles never falls below 50 % across the entire parameter range studied here, leading to the aforementioned ratio being constant.

The size distribution of clusters can be found in Fig. 4. Here, we plot a probability distribution function (PDF) of finding clusters of a given size. Fig. 4(a) corresponds to $B_0^* = 0$ and shows the PDFs for three different area fractions: $\phi_n = 0.175$, 0.210, and 0.315. As the area fraction increases, larger clusters become more likely, as evidenced by the heavier tail of the green ($\phi_n = 0.175$) PDF at higher cluster sizes; however, their topology does not change, as previously seen in Fig. 1. The distributions show bi-exponential decay, indicating that the system is close to the percolation threshold.

Comparing Fig. 4(b) and (c), one can conclude that while the PDFs for B_0^* and B_1^* remain quite similar, the decay of the PDF for B_2^* is markedly steeper. The latter also exhibits the strongest sensitivity to the area fraction: at low ϕ_m, Fig. 4(b), almost no clusters with more than 10 particles are observed, and the decay follows a single-exponential form apart from a statistically noisy tail at large cluster sizes. In contrast, at high ϕ_m, Fig. 4(c), the difference between the B_0^* and B_2^* PDFs becomes much less pronounced.

In summary, this subsection demonstrates that for the system parameters considered above, increasing the area fraction promotes the formation of larger clusters but does not have a significant impact

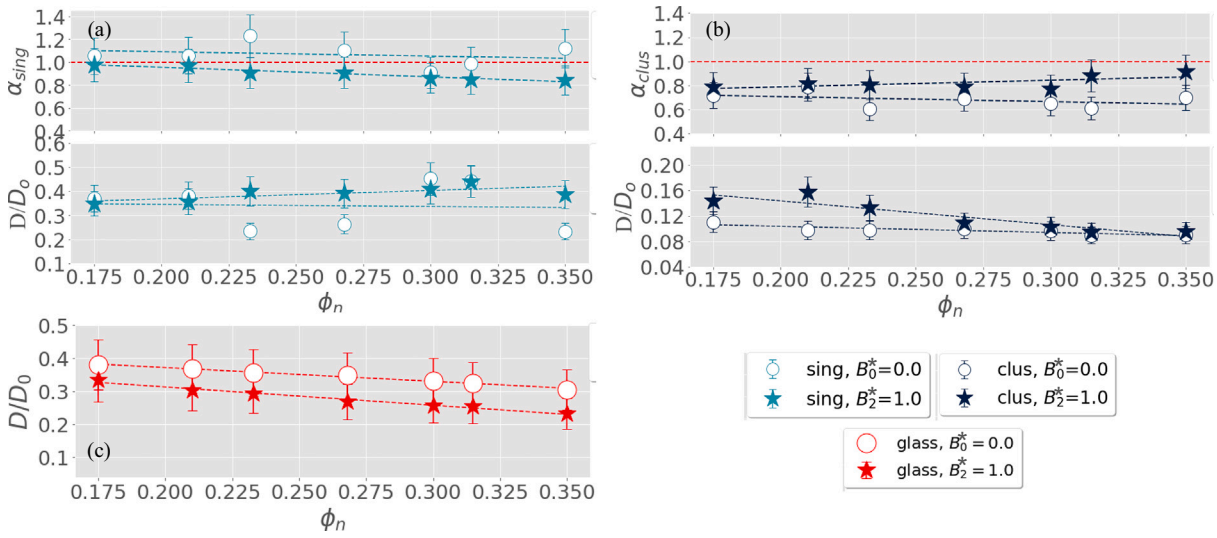

Fig. 5. The scaling exponent, α, Eq. (7), in upper panels and effective diffusion coefficient, D/D_0 in lower panels, versus ϕ_n. The values of magnetic induction are provided in the legend. (a) single (nonaggregated) magnetic particles; (b) magnetic particles in clusters; (c) nonmagnetic particles (glass), $\alpha = 1$ for all ϕ_n and is not plotted here.

under zero applied induction, as the system is highly aggregated and the fraction of single particles is negligible in agreement with the previous observations in work [47]. The magnetic induction hinders the formation of large clusters. This effect is more pronounced at low area fractions. At a high area fraction of particles, the density effects dominate over an applied induction.

As ϕ_n increases, the system approaches and eventually reaches the percolation threshold, where clusters span the entire system [48]. For the parameters considered here, however, no percolation has been observed.

Such clustering behaviour cannot help but affect self-diffusion in the layer of a model ferrogranulate; therefore, in the next subsection, we analyse the mean-square displacement of both Stockmayer and purely repulsive beads.

3.2. Self-diffusion

Using mean-squared displacement and Eq. (7), we estimated the diffusion coefficients, D, and exponents α for single magnetic particles, magnetic particles in clusters, and glass particles. The results are collected in Fig. 5.

In the lower panel of Fig. 5(a), we show the normalised self-diffusion coefficient, D/D_0, of single magnetic particles at low induction B_0^* (circles) and high induction B_2^* (stars) as a function of the total area fraction ϕ_n. The straight lines correspond to linear fits. The results demonstrate that the magnitude of the diffusion coefficient remains essentially unchanged: neither the applied magnetic induction nor increasing ϕ_n has a noticeable effect on the self-diffusion speed of isolated particles. In contrast, the exponent α, displayed in the upper panel of the same figure, is sensitive to both ϕ_n and B_2^*. At zero induction, the particles exhibit normal diffusive behaviour ($\alpha \approx 1$) over the entire range of area fractions. Under strong magnetic induction, however, their motion becomes progressively subdiffusive, with α decreasing to approximately 0.8 at the highest ϕ_n. This trend arises because single particles become predominantly aligned along the direction of the induction - orthogonal to the layer and parallel to one another - resulting in strong dipolar repulsion that suppresses normal diffusion. Thus, although the diffusion coefficient itself remains robust, the nature of the particle trajectories is substantially altered by the combined influence of the increasing area fraction and applied induction.

Magnetic particles within clusters experience the joint effects of crowding and induction even more strongly. As shown in Fig. 5(b), the ratio D/D_0 is significantly lower for clustered particles than for single ones, and it decreases further as both the induction (B_2^*, stars) and ϕ_n increase.

As discussed in the previous section, this behaviour reflects the reduced effectiveness of the orthogonal induction at higher ϕ_n, where dipolar interactions promoting in-plane chain formation dominate the dynamics. For the same reason, D/D_0 remains low even in the absence of induction (B_0^*, circles): under these conditions, clusters are already large, and most particles are aggregated regardless of ϕ_n, as illustrated in Figs. 2 and 3. The largest difference between circles and squares (B_0^* and B_0^*) in the values of D/D_0 is observed for low area fractions, where the ratio of particles in clusters, as shown in Fig. 3, is almost an order of magnitude. This significant difference, however, results in only a 25 % decrease in the diffusion coefficient, highlighting the strongly nonlinear relationship between clustering and diffusivity. No ϕ_n dependence is measured for D/D_0 in the case of B_0^* (circles). The resulting ϕ_n-independent cluster-size distribution at B_0^* (Fig. 4) explains the nearly constant trend observed for D/D_0. As for the values of α, the particles in clusters clearly exhibit subdiffusion.

It is particularly interesting to examine the behaviour of purely repulsive, non-dipolar particles. Even though the value of α remains very close to one (see Supplementary Information), the diffusion coefficient turns out to be not only ϕ_n-dependent but also sensitive to the applied magnetic induction. As shown in Fig. 5(c), the values of D/D_0 for B_0^* (circles) and B_2^* (stars) differ markedly: the latter is consistently lower across the entire range of ϕ_n. This effect arises from the repulsion between the isolated magnetic particles discussed above, which substantially restricts the space available for the non-magnetic particles to diffuse. In this sense, one may view the phenomenon as a kind of magnetic “cooling” of a non-magnetic component. Note that non-magnetic spheres are analogous to the glass spheres dispersed in a ferrogranulate, where similar cooling effects may, in principle, be observable experimentally.

3.3. Non-Gaussianity of particle displacements

The final step in our analysis is to determine whether any of the diffusion processes modelled here are non-Gaussian. To examine this, we calculate the probability that a particle (either a single magnetic particle, a glass particle, or a magnetic particle within a cluster) moves by a distance δx during a time interval τ. We consider five different time intervals, measured in simulation units,

$$\tau_i \in \{0.5,\ 1,\ 2,\ 2.5,\ 5\}, \qquad i = 1 \ldots 5.$$

The shortest interval, τ_1, corresponds to the ballistic regime. All intermediate values, except for the last one, lie within the intermediate regime, while τ_5 captures the diffusive part of the MSD (see Fig. S2 in the Supplementary Information).

Next, we compute the non-Gaussianity parameter (Fisher's coefficient), defined using the fourth moment $\langle\mu_4\rangle$ and the second moment μ_2 of the displacement distribution:

$$\gamma_2 = \frac{\mu_4}{\mu_2^2} - 3. \tag{9}$$

A distribution close to a normal yields $\gamma_2 \approx 0$. Positive values indicate a leptokurtic distribution, whereas negative values correspond to a platykurtic one [49].

In the absence of an applied induction, B_0^*, the values of γ_2 for the few non-aggregated magnetic particles remain close to zero, independently of the system area fraction. The raw data for the frequencies of different displacements can be found in the supplementary materials, Fig. S3. The values of γ_2 change markedly in the case of a strong applied induction, B_2^*, as shown in Fig. 6(a). For each value of τ, three columns correspond to three different area fractions, increasing from the lowest (ϕ_1, leftmost) to the highest (ϕ_8, rightmost).

For a fixed ϕ_n, the non-Gaussianity increases monotonically with increasing displacement. Interestingly, in the ballistic and intermediate regimes (τ_1–τ_4), the value of γ_2 for the intermediate area fraction ϕ_4 exceeds that for ϕ_8. We attribute this to the higher fraction of single magnetic particles at ϕ_4, as shown in Fig. 2. Since γ_2 reflects the strength of interactions, a larger population of individual magnetic particles with dipoles aligned with the applied induction leads to stronger effects of dipolar repulsion on a short timescale.

In the diffusive regime, however, the diffusion exponent α decreases monotonically with ϕ_n, indicating crowding-induced subdiffusivity (see Fig. 5(a)). At these longer time scales, the non-Gaussianity also becomes a monotonic function of ϕ_n.

In Fig. 6(b), one can see that magnetic particles in clusters exhibit a strongly non-Gaussian displacement distribution (actual distributions are shown in Supplementary Fig. S4). Here, for each τ_i, one finds six columns: the first three are for B_0^*, and the other three are for B_2^*. Analogously to Fig. 6(a), the three columns for each induction value from left to right correspond to ϕ_1, ϕ_4, and ϕ_8. For short time-scales (ballistic or nearly ballistic intervals of τ_1 and τ_2), neither the induction nor the area fraction has notable effects on γ_2.

The situation changes for τ_3 and τ_4. Here, the values of γ_2 reflect the internal dynamical heterogeneity of the aggregates. When the magnetic field is applied orthogonally to the substrate, it destabilises planar clustering and suppresses all but the most favourable dipole-dipole arrangements, resulting in tight, highly constrained clusters that are typically smaller than those formed in zero field. At intermediate lag times, this produces a monotonic increase in non-Gaussianity with increasing ϕ_n, since higher area fractions enhance the internal restrictions within these tight surviving aggregates. In contrast, the clusters in zero field are larger and structurally more variable; their internal rearrangements are most heterogeneous at intermediate ϕ_n, leading to a non-monotonic dependence of γ_2.

At long lag times, τ_5, both zero and applied induction values exhibit non-monotonic behaviour again, albeit for different reasons. The small, tight field-stabilised clusters relax and reorganise sufficiently to reduce their internal heterogeneity at the highest ϕ_n, whereas the large zero-field clusters, although loosely structured, occupy appreciably more space and provide a greater number of neighbours that constrain long displacements. This increased spatial crowding leads to an analogous reduction in γ_2 at high ϕ_n in the diffusive regime.

Finally, in Fig. 6(c) we observe that the applied magnetic induction also influences the values of γ_2 calculated for the displacements of the purely repulsive, non-magnetic particles (akin to the glass beads in ferrogranulates). As confirmed by the raw distributions provided in the Supplementary Fig. S5, at B_0^* the displacement statistics of these non-magnetic particles remain practically Gaussian for all but the highest area fraction: only at ϕ_8 and at the longest lag time τ_5 does a modest deviation from Gaussianity appear. In contrast, at B_2^* the values of γ_2 are no longer negligible. Instead, γ_2 increases markedly with both ϕ_n and τ_i, in some cases even exceeding the non-Gaussianity observed for isolated magnetic particles in Fig. 6(a). This enhanced heterogeneity arises because the field-induced restructuring of the magnetic particles modifies the local environment experienced by the non-magnetic ones: the formation of compact dipolar aggregates creates spatially extended obstacles and transient cages, leading to intermittent trapping, uneven free volumes, and thus a strongly non-Gaussian displacement distribution for the repulsive particles.

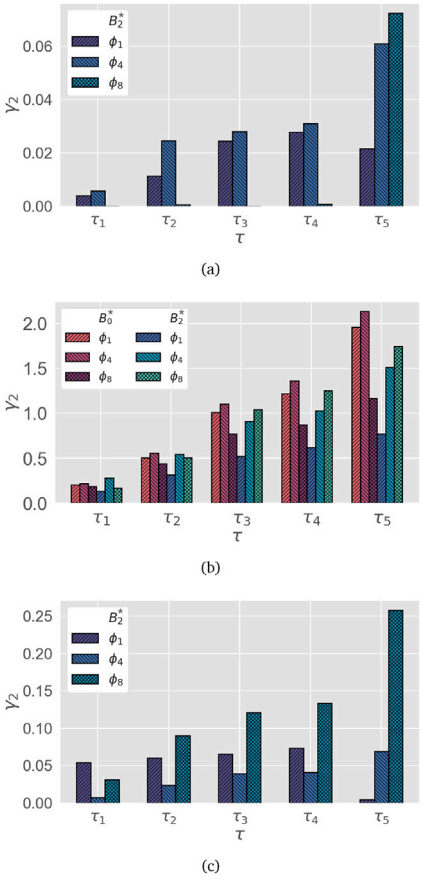

Fig. 6. Non-Gaussian parameter γ_2 for (a) single (nonaggregated) magnetic particles, (b) magnetic particles within clusters, and (c) purely repulsive non-magnetic particles, shown for several lag times τ_i. For each panel, the bars correspond to different area fractions, and colours indicate either zero induction, B_0^*, or strong applied induction, B_2^* (in (b)). Raw displacement distributions are provided in the Supplementary Information (Figs. S3–S5).

4. Conclusions

In this work, we have carried out a systematic numerical study of a quasi-two-dimensional mixed system composed of Stockmayer-type dipolar particles and purely repulsive non-polar particles, motivated by the broader goal of understanding transport processes in ferrogranular layers. By combining detailed cluster analysis with a quantitative evaluation of self-diffusion, we have demonstrated how the interplay between particle area fraction, dipolar interactions, and an out-of-plane magnetic induction governs the structural organisation and dynamical behaviour of the mixture.

Our results show that increasing the total area fraction enhances clustering among magnetic particles, although the topology of the clusters remains qualitatively unchanged. The application of an external magnetic induction reduces cluster sizes by promoting out-of-plane alignment and dipolar repulsion between single particles. This effect is most pronounced at low area fractions; whereas, at high area fractions, dipolar interactions diminish the influence of the induction, leading to similar cluster statistics across field strengths. Importantly, the system remains below the percolation threshold for all parameter sets explored.

The cluster morphology has direct consequences for the particle mobility. Isolated magnetic particles retain a diffusion coefficient that is largely independent of induction and concentration, but their motion becomes increasingly subdiffusive under strong induction. Magnetic particles embedded in clusters diffuse substantially more slowly and exhibit clear subdiffusive dynamics, reflecting the constrained motion imposed by dense bundles of chain-like aggregates. Remarkably, even the purely repulsive non-magnetic particles – despite exhibiting nearly Brownian displacement statistics – display diffusion coefficients that are strongly suppressed by magnetic induction.

We showed that the interplay between magnetic induction and increasing area fraction strongly influences the average particle displacement distribution in the system. As expected, magnetic particles within clusters display consistently non-Gaussian dynamics, which become more pronounced with both area fraction and applied field (on short-time scales). Our displacement analysis reveals that, in the absence of induction, isolated magnetic particles diffuse essentially in a Gaussian manner across all concentrations. Under strong induction, however, the dynamics become increasingly non-Gaussian, with the non-Gaussianity parameter rising with displacement and showing a marked dependence on particle concentration. At intermediate area fractions, where the proportion of single magnetic particles is higher, short-time dynamics exhibit enhanced non-Gaussianity due to the stronger influence of dipolar repulsion. At longer time scales, by contrast, the system enters a crowding-dominated diffusive regime, in which both the diffusion exponent and the non-Gaussianity vary monotonically with area fraction. At sufficiently high induction and crowding, even the glass particles develop non-Gaussian dynamics, confirming field-driven dynamical cooling of the non-magnetic component.

Altogether, our findings reveal the rich and highly nonlinear coupling between dipolar interactions, cluster formation, and transport in mixed quasi-2D dipolar systems. The study provides a framework for interpreting diffusion phenomena in ferrogranular materials and paves the way for future experimental verification, particularly regarding induction-controlled cooling of non-magnetic components. Extensions of this work may include time-dependent fields, polydispersity effects, or direct comparisons with trajectory-resolved experimental data from granular magnetic layers.

CRediT authorship contribution statement

Oksana Bilous: Investigation, Visualization. **Kirill A. Okrugin:** Conceptualization, Software. **Ali Lakkis:** Visualization, Data curation. **Reinhard Richter:** Review, Editing, Funding acquisition. **Sofia Kantorovich:** Writing – review & editing, Conceptualization, Supervision, Funding acquisition.

Declaration of competing interest

The authors declare the following financial interests/personal relationships which may be considered as potential competing interests:

Sofia Kantorovich reports that financial support was provided by the University of Vienna. If there are other authors, they declare that they have no known competing financial interests or personal relationships that could have appeared to influence the work reported in this paper.

Acknowledgments

The authors express their gratitude to **Dr. Pedro A. Sánchez** and **Dr. Andrey Kuznetsov** for the enlightening and clarifying discussions. The research was supported by the German-Austrian (D-A) research project funded by DFG (Ri 1054/7) and FWF (I5160). All simulations were performed in VSC4 (Vienna Scientific Cluster).

Appendix A. Supplementary data

Supplementary data to this article can be found online at doi:10.1016/j.molliq.2025.129210.

Data availability

Data will be made available on request.

References

[1] A. Einstein, Über die von DER molekularkinetischen theorie DER wärme geforderte bewegung von in ruhenden flüssigkeiten suspendierten teilchen, Ann. Phys. (Berlin) 4 (1905), https://doi.org/10.1002/andp.19053220806
[2] M. Smoluchowski, The kinetic theory of brownian molecular motion and suspensions, Ann. Phys. (Berlin) 21 (1906) 756–780, https://doi.org/10.1002/andp.19063261405
[3] J.C. Slattery, R.B. Bird, Calculation of the diffusion coefficient of dilute gases and of the self-diffusion coefficient of dense gases, AIChE J. 4 (1958) 137–142, https://doi.org/10.1002/aic.690040205
[4] M. Mantina, Y. Wang, R. Arroyave, L.Q. Chen, Z.K. Liu, C. Wolverton, First-principles calculation of self-diffusion coefficients, Phys. Rev. Lett. 100 (2008) 215901, https://doi.org/10.1103/PhysRevLett.100.215901
[5] I.N. Tsimpanogiannis, O.A. Moultos, L.F.M. Franco, M.B.D.M. Spera, M. Erdös, I.G. Economou, Self-diffusion coefficient of bulk and confined water: a critical review of classical molecular simulation studies, Mol. Simul. 45 (2019) 425–453, https://doi.org/10.1080/08927022.2018.1511903
[6] J. Busch, D. Paschek, Computing accurate true self-diffusion coefficients and shear viscosities using the orthoboxy approach, J. Phys. Chem. B 128 (2024) 1040–1052, https://doi.org/10.1021/acs.jpcb.3c07540
[7] K. Zahn, J.M. Méndez-Alcaraz, G. Maret, Hydrodynamic interactions may enhance the self-diffusion of colloidal particles, Phys. Rev. Lett. 79 (1997) 175, https://doi.org/10.1103/PhysRevLett.79.175
[8] S.D. Bembenek, G. Szamel, The role of attractive interactions in self-diffusion, J. Phys. Chem. B 104 (2000) 10647–10652, https://doi.org/10.1021/jp0025835
[9] F. Roosen-Runge, P. Schurtenberger, A. Stradner, Self-diffusion of nonspherical particles fundamentally conflicts with effective sphere models, J. Phys.: Condens. Matter 33 (2021) 154002, https://doi.org/10.1088/1361-648X/abdff9
[10] R.M. Noyes, Models relating molecular reactivity and diffusion in liquids, J. Am. Chem. Soc. 78 (1956) 5486–5490, https://doi.org/10.1021/ja01602a007
[11] J.R. Sangoro, C. Iacob, S. Naumov, R. Valiullin, H. Rexhausen, J. Hunger, R. Buchner, V. Strehmel, J. Kärger, F. Kremer, Diffusion in ionic liquids: the interplay between molecular structure and dynamics, Soft Matter 7 (2011) 1678–1681, https://doi.org/10.1039/C0SM01404D
[12] W.H. Stockmayer, Second virial coefficients of polar gases, J. Chem. Phys. 9 (1941) 398–402, https://doi.org/10.1063/1.1750922
[13] J.S. Rowlinson, The third virial coefficients of polar gases, J. Chem. Phys. 19 (1951) 827–831, https://doi.org/10.1063/1.1748390
[14] M.E. Van Leeuwen, B. Smit, E.M. Hendriks, Vapour-liquid equilibria of Stockmayer fluids, Mol. Phys. 78 (1993) 271–283, https://doi.org/10.1080/00268979300100231
[15] B. Groh, S. Dietrich, Ferroelectric phase in Stockmayer fluids, Phys. Rev. E 50 (1994) 3814, https://doi.org/10.1103/PhysRevE.50.3814
[16] M.J. Stevens, G.S. Grest, Phase coexistence of a stockmayer fluid in an applied field, Phys. Rev. E 51 (1995) 5976, https://doi.org/10.1103/PhysRevE.51.5976
[17] C. Spöler, S.H.L. Klapp, Phase behavior of stockmayer fluids confined to a nonpolar porous material, J. Chem. Phys. 118 (2003) 3628–3638, https://doi.org/10.1063/1.1539047
[18] J. Bartke, R. Hentschke, Phase behavior of the stockmayer fluid via molecular dynamics simulation, Phys. Rev. E 75 (2007) 061503, https://doi.org/10.1103/PhysRevE.75.061503
[19] J. Bartke, Computer Simulation of the Stockmayer Fluid (Ph.D. thesis), Wuppertal, 2008.
[20] E.A. Elfimova, A.O. Ivanov, J.O. Sindt, P.J. Camp, Thermodynamics of the stockmayer fluid in an applied field, Mol. Phys. 113 (2015) 3717–3728, https://doi.org/10.1080/00268976.2015.1058979
[21] J. Marx, M. Kohns, K. Langenbach, Systematic study of vapour–liquid equilibria in binary mixtures of fluids with different polarity from molecular simulations, Mol. Phys. 120 (2022) e2141150, https://doi.org/10.1080/00268976.2022.2141150
[22] D.L. Blair, A. Kudrolli, Clustering transitions in vibrofluidized magnetized granular materials, Phys. Rev. E 67 (2003) 021302, https://doi.org/10.1103/PhysRevE.67.021302
[23] K. Son, Y. Choe, E. Kwon, L.G. Rigon, Y. Baek, H.-Y. Kim, Dynamics of self-propelled particles in vibrated dense granular media, Soft Matter 20 (2024) 2777–2788, https://doi.org/10.1039/D3SM01596C

[24] P.A. Sánchez, J. Miller, S.S. Kantorovich, R. Richter, Unknotting of quasi-two-dimensional ferrogranular networks by in-plane homogeneous magnetic fields, J. Magn. Magn. Mater. 499 (2020) 166182, https://doi.org/10.1016/j.jmmm.2019.166182
[25] A. Lakkis, M. Biersack, O. Bilous, S. Kantorovich, R. Richter, Controlling the coarsening dynamics of ferrogranulate networks by means of the filling fraction—less is more susceptible, J. Magn. Magn. Mater. 589 (2024) 171620, https://doi.org/10.1016/j.jmmm.2023.171620
[26] O. Bilous, K.A. Okrugin, A. Lakkis, M. Biersack, R. Richter, S. Kantorovich, In silico study of area fraction effects on the behaviour of a ferrogranulate layer in an orthogonal applied field, J. Magn. Magn. Mater. 589 (2024) 171627, https://doi.org/10.1016/j.jmmm.2023.171627
[27] K. Šolc, W.H. Stockmayer, Kinetics of diffusion-controlled reaction between chemically asymmetric molecules. II. Approximate steady-state solution, Int. J. Chem. Kinet. 5 (1973) 733–752, https://doi.org/10.1002/kin.550050503
[28] L. Perera, M.L. Berkowitz, Dynamics of ION solvation in a stockmayer fluid, J. Chem. Phys. 96 (1992) 3092–3101, https://doi.org/10.1063/1.461954
[29] V.M. Buzmakov, A.F. Pshenichnikov, On the structure of microaggregates in magnetite colloids, J. Colloid Interface Sci. 182 (1996) 63–70, https://doi.org/10.1006/jcis.1996.0437
[30] A.S. Ivanov, A.F. Pshenichnikov, Magnetophoresis and diffusion of colloidal particles in a thin layer of magnetic fluids, J. Magn. Magn. Mater. 322 (2010) 2575–2580, https://doi.org/10.1016/j.jmmm.2010.03.023
[31] A.F. Pshenichnikov, E.A. Elfimova, A.O. Ivanov, Magnetophoresis, sedimentation, and diffusion of particles in concentrated magnetic fluids, J. Chem. Phys. 134 (2011), https://doi.org/10.1063/1.3586806
[32] A.B. Dobroserdova, S.S. Kantorovich, Self-diffusion in monodisperse three-dimensional magnetic fluids by molecular dynamics simulations, J. Magn. Magn. Mater. 431 (2017) 176–179, https://doi.org/10.1016/j.jmmm.2016.09.117
[33] M. Hod, A. Dobroserdova, S. Samin, C. Dobbrow, A.M. Schmidt, M. Gottlieb, S. Kantorovich, Dilution effects on combined magnetic and electric dipole interactions: a study of ferromagnetic cobalt nanoparticles with tuneable interactions, J. Chem. Phys. 147 (2017), https://doi.org/10.1063/1.4995428
[34] A.B. Dobroserdova, S.S. Kantorovich, Self-diffusion in bidisperse systems of magnetic nanoparticles, Phys. Rev. E 103 (2021) 012612, https://doi.org/10.1103/PhysRevE.103.012612
[35] A. Kögel, P.A. Sánchez, R. Maretzki, T. Dumont, E.S. Pyanzina, S.S. Kantorovich, R. Richter, Coarsening dynamics of ferromagnetic networks — experimental results and simulations, Soft Matter 14 (2018) 1001–1015, https://doi.org/10.1039/C7SM00796E
[36] J.D. Weeks, D. Chandler, H.C. Andersen, Role of repulsive forces in determining the equilibrium structure of simple liquids, J. Chem. Phys. 54 (1971) 5237–5247, https://doi.org/10.1063/1.1674820
[37] M. Biersack, A. Lakkis, R. Richter, O. Bilous, P.A. Sánchez, S.S. Kantorovich, Controlling the coarsening dynamics of ferrogranular networks by means of a vertical magnetic field, Phys. Rev. E 108 (2023) 054905, https://doi.org/10.1103/PhysRevE.108.054905
[38] C. Holm, A. Ivanov, S. Kantorovich, E. Pyanzina, E. Reznikov, Equilibrium properties of a bidisperse ferrofluid with chain aggregates: theory and computer simulations, J. Phys.: Condens. Matter 18 (2006) S2737, https://doi.org/10.1088/0953-8984/18/38/S14
[39] A. Arnold, O. Lenz, S. Kesselheim, R. Weeber, F. Fahrenberger, D. Roehm, P. Košovan, C. Holm, ESPResSo 3.1: molecular dynamics software for coarse-grained models, In M. Griebel, M.A. Schweitzer (Eds.), Meshfree Methods for Partial Differential Equations VI, Volume 89 of Lecture Notes in Computational Science and Engineering, Springer Berlin Heidelberg, 2013, pp. 1–23, https://doi.org/10.1007/978-3-642-32979-1_1
[40] J.J. Cerdà, V. Ballenegger, O. Lenz, C. Holm, P3m algorithm for dipolar interactions, J. Chem. Phys. 129 (2008) 234104, https://doi.org/10.1063/1.3000389
[41] A. Bródka, Ewald summation method with electrostatic layer correction for interactions of point dipoles in slab geometry, Chem. Phys. Lett. 400 (2004) 62–67, https://doi.org/10.1016/j.cplett.2004.10.086
[42] P. de Buyl, Tidynamics: a tiny package to compute the dynamics of stochastic and molecular simulations, J. Open Source Softw. 3 (2018) 877, https://doi.org/10.21105/joss.00877
[43] A.V. Chechkin, F. Seno, R. Metzler, I.M. Sokolov, Brownian yet non-gaussian diffusion: from superstatistics to subordination of diffusing diffusivities, Phys. Rev. X 7 (2017) 021002, https://doi.org/10.1103/PhysRevX.7.021002
[44] S. Egri, G. Bihari, Self-assembly of magnetic spheres: a new experimental method and related theory, J. Phys. Commun. 2 (2018) 105003, https://doi.org/10.1088/2399-6528/aadfc9
[45] H. Carstensen, A. Krämer, V. Kapaklis, M. Wolff, Self-assembly and percolation in two-dimensional binary magnetic colloids, Soft Matter 18 (2022) 6222–6228, https://doi.org/10.1039/D2SM00661H
[46] E. Navarro, C. Falcón, Statistics of a granular cluster ensemble at a liquid-solid-like phase transition, Phys. Rev. E 109 (2024) 054901, https://doi.org/10.1103/PhysRevE.109.054901
[47] A. Wafflard, E. Opsomer, N. Vandewalle, Dipolar gels formed by aggregation of magnetized beads, Phys. Rev. E 110 (2024) 054608, https://doi.org/10.1103/PhysRevE.110.054608
[48] L. Rovigatti, J. Russo, F. Sciortino, Structural properties of the dipolar hard-sphere fluid at low temperatures and densities, Soft Matter 8 (2012) 6310–6319, https://doi.org/10.1039/C2SM25192B
[49] M. Jambu, Chapter 3 - 1-d statistical data analysis, In M. Jambu (Ed.), Exploratory and Multivariate Data Analysis, Academic Press, Boston, 1991, pp. 27–62, https://doi.org/10.1016/B978-0-08-092367-3.50007-1